



Preparation of magnetically recoverable Fe₃O₄–graphene oxide catalyst by green method and its application for reduction of nitropyrimidine in aqueous medium

Mahdieh Namvar-Mahboub¹ · Elaheh Khodeir¹ · Azam Karimian²

Received: 23 January 2018 / Accepted: 9 July 2018
© Springer Nature B.V. 2018

Abstract

Magnetic graphene oxide (GO)/amino-functionalized Fe₃O₄ nanocomposite was prepared using tannic acid as binder. For this purpose, Fe₃O₄ nanoparticles were modified by phenylenediamine and GO was partially reduced and modified in presence of tannic acid. Nanocomposites were prepared under three different synthesis conditions. The morphology and chemical structure of the magnetic GO nanocomposites were studied by means of Fourier-transform infrared spectroscopy, X-ray powder diffraction, transmission electron microscopy, scanning electron microscopy, thermogravimetric analysis, and vibrating-sample magnetometry. The catalytic activity of the optimal GO/Fe₃O₄ nanocomposite was then studied using reduction of 2,4-dichloro-6-methyl-5-nitropyrimidine at different catalyst doses. The reaction time was probed using ultraviolet–visible (UV–Vis) absorption spectroscopy and thin-layer chromatography (TLC) analysis. The results demonstrated that, on increasing the catalyst dose from 1 to 7 mg, the reaction time decreased from 20 to 5 min. The synthesized product was also confirmed by nuclear magnetic resonance. The very low catalyst dose required, green media, and low temperature demonstrate that the as-prepared magnetic GO catalyst has high catalytic activity for reduction of nitropyrimidine to aminopyrimidine in aqueous medium.

Keywords Magnetic GO · Catalysis · Nanocomposite · Reduction reaction

✉ Mahdieh Namvar-Mahboub
Namvar@gonabad.ac.ir; namvarmahboob@yahoo.com

¹ Department of Chemical Engineering, University of Gonabad, Gonabad, Iran

² Department of Chemistry, University of Gonabad, Gonabad, Iran

Introduction

Aminopyrimidines are a group of key intermediate compounds employed to produce many marketed drugs such as nucleoside antibiotics, antiinflammatory drugs, and antibacterial and cardiovascular agents, owing to their biological properties [1, 2]. There are various protocols to synthesize these compounds, including one-pot synthesis from ketones, arylacetylenes, and guanidines [2], reduction of nitro compounds [3, 4], etc. However, development of highly selective, low-cost, easily scalable, and safe methods remains a major challenge for design of appropriate and economical production lines. Based on literature reports, it seems that synthetic transformation of nitropyrimidines to aminopyrimidines in presence of suitable reagents via reduction reaction can meet the mentioned conditions [4–6]. Regarding industrial aspects, application of a nontoxic, stable, highly active catalyst is essential for the above-mentioned organic synthesis. In this regard, carbon-based catalysts such as graphene, its derivatives, and hybrid forms have been considered as environmentally friendly catalysts and/or adsorbents over recent decades [7].

GO is one of the graphene derivatives which has abundant oxygenated functional groups, including hydroxyl and epoxy groups (both on the basal plane) as well as carbonyl and carboxyl groups (both at sheet edges). The mentioned functional groups are responsible for its high hydrophilicity. The two-dimensional lamellar structure and high surface area accompanied with full accessibility and edge reactivity make it favorable for assembly of graphene-based hybrid nanomaterials [8–11]. Over the past decade, GO-based nanocomposites have been considered as potential materials for applications such as drug delivery [12–14], water purification [15, 16], catalytic processes [7, 17–19], biosensing [20, 21], polymer composites [22], etc. To date, depending on the application, different substances including Pd [23], Pt [24], Au [25], Ag [26], TiO₂ [27], SnO₂ [28], Fe₃O₄ [29], and Co-Fe₂O₄ [30] have been assembled onto inorganic GO sheets to obtain nanocomposites with novel or enhanced properties. Among GO nanocomposites with catalytic applications, GO-Fe₃O₄ has drawn attention from researchers due to the biocompatibility and catalytic activity of Fe₃O₄, as well as its magnetic property, which simplifies separation of such nanocatalysts from the reaction system using an external magnetic field. To date, the catalytic activity of magnetic GO nanocomposite has been studied for reduction of nitrophenol [31, 32], oxidation of 2,4 dichlorophenol [33], Suzuki and Heck cross-coupling reactions [19], and A³ coupling reaction of aldehyde, amine, and alkyne [34].

Commonly, Fe₃O₄ nanoparticles can attach to a GO layer via in situ reduction of iron salt precursors [19, 35–38]. In this case, magnetite may be physically adsorbed on the GO surface or via electrostatic interaction. This method faces major challenges, including high synthetic temperature, difficulty in controlling the Fe₃O₄ loading, weak GO-Fe₃O₄ interaction, and leaching of magnetic nanoparticles [35, 36]. Accordingly, in recent years, covalent attachment of Fe₃O₄ nanoparticles onto GO has been developed to obtain nanocomposites with high stability and better performance [12, 29, 39]; For instance, He et al. [29] reported fabrication of an Fe₃O₄/GO nanocomposite using a covalent process. They modified Fe₃O₄ using

tetraethylorthosilicate and (3-aminopropyl)triethoxysilane to react with the carboxylic groups of GO with the aid of 1-ethyl-3-(3-dimethylaminopropyl)carbodiimide (EDC) and *N*-hydroxysuccinimide (NHS). In addition, Li et al. [39] used EDC and NHS to form carboxamide bonds between amino groups of Fe₃O₄/SiO₂ core-shell nanoparticles and carboxylic groups of GO. Xi et al. [36] loaded amino-modified Fe₃O₄ nanoparticles onto the surface of GO sheets. They functionalized GO sheets by SOCl₂ to obtain GO with acid chloride groups, which can react with amino groups of modified Fe₃O₄. Yang et al. [12] prepared a magnetic GO nanocomposite by covalent attachment of dopamine-coated Fe₃O₄ and acyl chloride-functionalized GO. In all such literature reports, different chemical groups were introduced to achieve covalent attachment between magnetite and GO. Although reported results confirm appropriate covalent bonding, the multiplicity of toxic modifiers applied make such methods less desirable. It seems that use of nonhazardous attachment agents should be considered.

Accordingly, in the current study, we developed a novel, green method to prepare a covalently bonded GO-Fe₃O₄ nanocomposite, then studied its catalytic application. For this purpose, GO was modified in presence of tannic acid as reactive coating agent, then interacted with amino-functionalized magnetic nanoparticles through individual bonds, as probed by Fourier-transform infrared (FTIR) analysis. Additionally, the prepared magnetic nanocomposite was characterized by energy-dispersive X-ray spectroscopy (EDS), scanning electron microscopy (SEM), transmission electron microscopy (TEM), vibrating-sample magnetometry (VSM), and X-ray diffraction (XRD) analyses. The catalytic activity of the prepared magnetic GO nanoparticles was investigated via aminolysis reaction of 2,4-dichloro-6-methyl-5-nitropyrimidine in water as green solvent. The reaction time was probed at different catalyst doses, and the results compared with literature reports.

Materials and methods

Chemicals

Graphene oxide powder (99%) with average particle size of 40 nm and Fe₃O₄ nanoparticles (99%, 20–40 nm) were supplied by USNANO Co. (USA). Tannic acid and 1,2-phenylenediamine used as modifiers and sodium borohydride (NaBH₄) were obtained from Sigma Aldrich. Methanol (Merck) and deionized water were used as solvents.

2,4-Dichloro-6-methyl-5-nitropyrimidine was synthesized in our laboratory according to the procedure reported by Karimian et al. [40]. Analytical TLC was performed on Merck DC precoated TLC plates with 0.25-mm Kieselgel 60 F254.

Amino functionalization of Fe₃O₄ nanoparticles

To create strong bonding between GO and Fe₃O₄ nanoparticles, both of them were functionalized with appropriate chemical groups. In this study, Fe₃O₄ nanoparticles

were amino-functionalized using phenylenediamine according to the following procedure: Firstly, 100 mg Fe_3O_4 was added to 20 ml methanol and stirred at 50 °C for 30 min. Then 100 mg phenylenediamine was added to the suspension. After 12 h, nanoparticles were centrifuged and rinsed several times with deionized water and ethanol to remove excess phenylenediamine. Finally, the resulting amino-functionalized nanoparticles were dried in oven at 70 °C.

Preparation of tannic acid-coated GO

GO nanosheets (5 mg) were suspended in 5 ml deionized water. Separately, 10 mg tannic acid was dissolved in 8 ml deionized water. These two solutions were mixed and stirred for 1 h at ambient temperature. Unreacted tannic acid was removed from functionalized GO by washing with deionized water, and the resulting modified GO was dried in oven at 70 °C.

Preparation of GO- Fe_3O_4 nanocomposite

Amino-functionalized Fe_3O_4 nanoparticles and TA-GO at a certain mass ratio were dispersed in deionized water and stirred at constant temperature for 60 h to ensure reaction completion. The as-prepared nanocomposite was then separated magnetically, rinsed with deionized water, and dried in oven at 70 °C. Using this procedure, three different nanocomposite samples were prepared under different conditions (Table 1).

Characterization of GO- Fe_3O_4 nanocomposite

To study the morphology of the as-prepared nanocomposites, transmission electron microscopy (Leo 912 AB, Germany) and scanning electron microscopy (Leo 1450VP, Germany) equipped with EDS analysis were applied. XRD analysis was conducted using an X-ray diffractometer with Cu K_α radiation ($\lambda = 1.541874 \text{ \AA}$) in the range from 9.995° and 70.005°. Chemical bonds of nanocomposite were investigated via FTIR analysis. FTIR spectra were collected using a Thermo Nicolet AVATAR 370 FT-IR (USA) in the range from 4000 to 400 cm^{-1} at resolution of 4 cm^{-1} . Vibrating-sample magnetometry (BHV-55, Riken, Japan) was used to determine the magnetic property of the as-prepared material at room temperature. Thermogravimetric analysis was carried out using a Shimadzu TGA-50 from 23 to 800 °C under air atmosphere.

Table 1 Synthesis conditions for GO- Fe_3O_4 nanocomposite samples

Sample code	Stirring temperature (°C)	GO/ Fe_3O_4 mass ratio
MGO-1	25	1:1
MGO-2	50	1:1
MGO-3	25	3:1

Catalytic reduction of 2,4-dichloro-6-methyl-5-nitropyrimidine

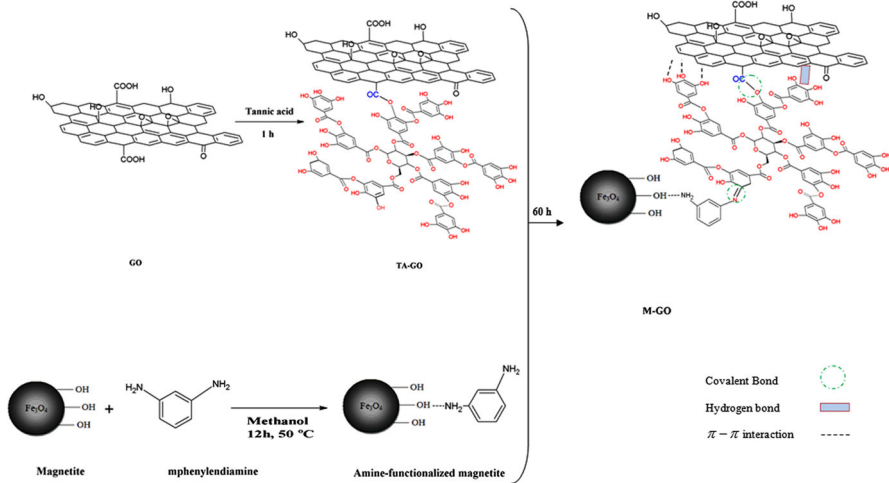
Reduction of 2,4-dichloro-6-methyl-5-nitropyrimidine was carried out in a conventional round-bottomed flask according to the following procedure: 15 mg (0.072 mmol) 2,4-dichloro-6-methyl-5-nitropyrimidine was dissolved in 5 ml deionized water. Then, 2.1 mmol NaBH₄ and different amounts (1, 3, 5, and 7 mg) of GO-Fe₃O₄ catalyst were added to the solution and stirred at ambient temperature. Sampling from the mixture was performed after 1, 5, and 10 min to monitor reaction progress via ultraviolet-visible (UV-Vis) spectrophotometry (Photonix Ar). For this purpose, each sample was diluted in deionized water. Adsorption spectra were collected in the range of 200–400 nm. The concentration change of 2,4-dichloro-6-methyl-5-aminopyrimidine was represented by the change of the adsorption peak at wavelength of 235 nm. In addition, reaction completion was confirmed by thin-layer chromatography (TLC) using chloroform/methanol (10:1) as eluent after 10 min. After reaction completion, the nanomagnetic catalyst was separated from the reaction mixture by applying an external magnetic field. To extract product from deionized water, 5 ml ethyl acetate (EtOAc) was added to the resultant solution. The organic phase was separated from water in decanter, dried over Na₂SO₄, and allowed to evaporate to give crude solid 2,4-dichloro-6-methylpyrimidin-5-amine in yield of 98% as red powder; m.p. 102–103 °C; ¹H NMR (CDCl₃): δ 2.32 (s, 3H, CH₃), 6.08 (s, 2H, NH₂, D₂O exchangeable); IR: ν 3472, 3371, 1621, 1555, 1527 cm⁻¹; MS (*m/z*) 178 (M⁺), 180 (M⁺ + 2). Anal. Calcd. for C₅H₅Cl₂N₃: C, 33.73; H, 2.83; N, 23.60. Found: C, 33.71; H, 2.83; N, 23.59.

Results and discussion

FTIR analysis of GO-Fe₃O₄ nanocomposite

The preparation procedure for the magnetic GO catalyst is described in Scheme 1, according to which it is expected that tannic acid will provide a large number of active sites leading to formation of covalent bonding, hydrogen bonding, and π-π interactions between TA-GO and amino-functionalized Fe₃O₄. FTIR analysis was carried out to confirm the chemical structure of each as-prepared nanocomposite, as presented in Scheme 1.

Figure 1a, b shows the FTIR spectra of tannic acid-functionalized-GO (TA-GO), NH₂-Fe₃O₄, and as-prepared magnetic nanocomposites, respectively. As seen from Fig. 1a, for TA-GO, the characteristic band at 3454 cm⁻¹ is ascribed to O-H stretching of GO. The bands at 2954 and 2912 cm⁻¹ correspond to symmetric and antisymmetric vibrations of CH₂. The band observed at 1764 cm⁻¹ can be assigned to stretching vibration of ester O=C=O in the structure of both GO and tannic acid. The band at 1078 cm⁻¹ corresponds to stretching vibration of ester C-O of tannic acid. The bands at 1627, 1444, 1288, and 900 cm⁻¹ correspond to stretching vibrations of aromatic C=C, stretching vibrations of esteric carbonyl groups, and stretching vibration of phenolic OH and γ(C-H) of aromatic rings [41–43]. In the case of amino-functionalized Fe₃O₄ (NH₂-Fe₃O₄), the strong band at 3457 cm⁻¹ is



Scheme 1 Preparation procedure for magnetic GO nanocomposite catalyst

attributed to stretching of NH₂ of amine group and OH group. The bands at 1604 and 1545 cm⁻¹ arise from deformations of water and bending of N–H, respectively. The band with strong intensity observed at 642 cm⁻¹ corresponds to Fe–O bond [44].

Figure 1b presents the FTIR spectra of the GO–Fe₃O₄ nanocomposites MGO-1, MGO-2, and MGO-3, revealing main characteristic bands of GO and Fe₃O₄ in the spectra for all three samples. The band at around 3500 cm⁻¹ is assigned to the overlap of amide groups of Fe₃O₄ and OH groups. Thus, the more intense band is observed when compared with that of GO. Moreover, the band intensity decreased with increasing GO/Fe₃O₄ ratio. Additionally, main characteristic bands of TA–GO and NH₂–Fe₃O₄ shifted to new values, confirming hydrogen bonding and π–π interaction between functionalized nanoparticles [34]. The aromatic carboxylic groups of tannic acid can also react with amine group of Fe₃O₄ [45–47]. In this case, characteristic band of C=N is observed at wavenumber of 1550 cm⁻¹. As can be seen, with increasing synthesis temperature, the intensity of the band at 640 cm⁻¹, corresponding to Fe–O, increased.

Morphology of as-prepared nanocomposite

TEM and SEM images of GO–Fe₃O₄ nanocomposite are shown in Fig. 2, clearly illustrating Fe₃O₄ nanoparticles distributed in GO nanosheets. The TEM images show magnetic nanoparticles with spherical structure and diameter of about 20 nm, anchored onto the surface of GO nanosheets. Additionally, the SEM image confirms presence of Fe₃O₄ nanoparticles, distinguished by their white color on GO sheets.

The EDS spectra and elemental analysis results for MGO-1 and MGO-3 are presented in Fig. 3. For both samples, peaks corresponding to Fe, O, and C were observed, indicating correct formation of GO–Fe₃O₄ nanocomposites. However, the

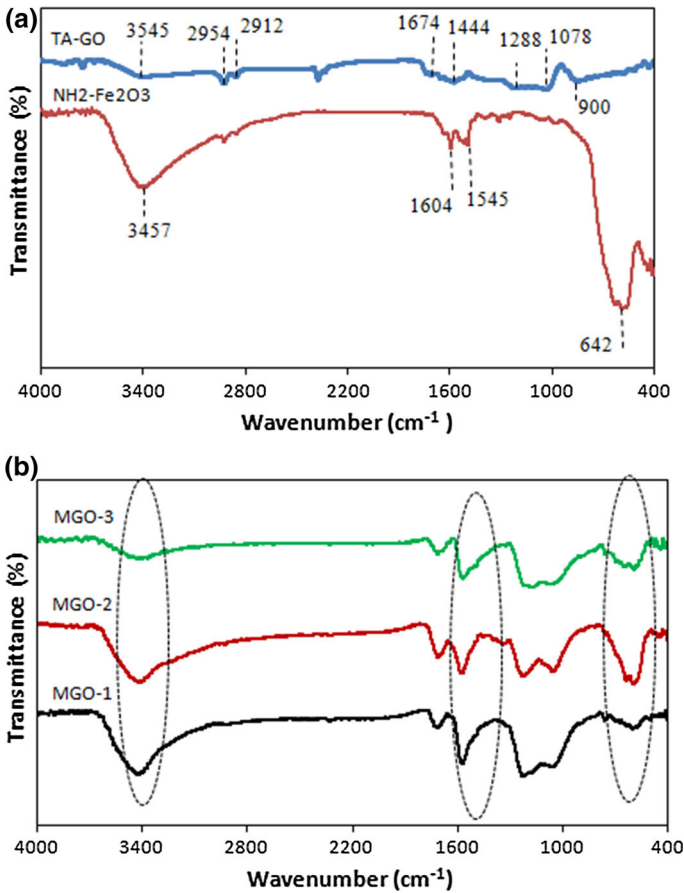


Fig. 1 FTIR spectra of **a** tannic acid-modified GO sample and amine-modified Fe₂O₃ nanoparticles, and **b** GO-Fe₃O₄ nanocomposites

Fe peak intensity decreased for MGO-3 compared with MGO-1. The elemental analysis data are consistent with the EDS results. As can be seen, the Fe content of MGO-2 was about 16.9%, while the Fe content of MGO-3 was about 4.1%. This trend can be ascribed to the reduction of the Fe₃O₄ dose in the initial solution for MGO-3.

The XRD patterns of GO-Fe₃O₄ nanocomposites obtained using different ratios of GO to Fe₃O₄ are presented in Fig. 4. For both MGO-1 and MGO-3, the original characteristic peak of GO can be observed at around 2θ of 11°, being related to (001) plane of GO [43]. Due to the interaction with metal oxide, the mentioned diffraction peak is broader for the GO nanocomposite compared with pure GO [34]. The peaks appearing at around 30°, 35°, 42°, 57°, and 63° are due to (220), (311), (400), (511), and (440) planes of Fe₃O₄ [48]. The presence of the above-mentioned peaks indicate that the nanocomposites show characteristic peaks of magnetite. As

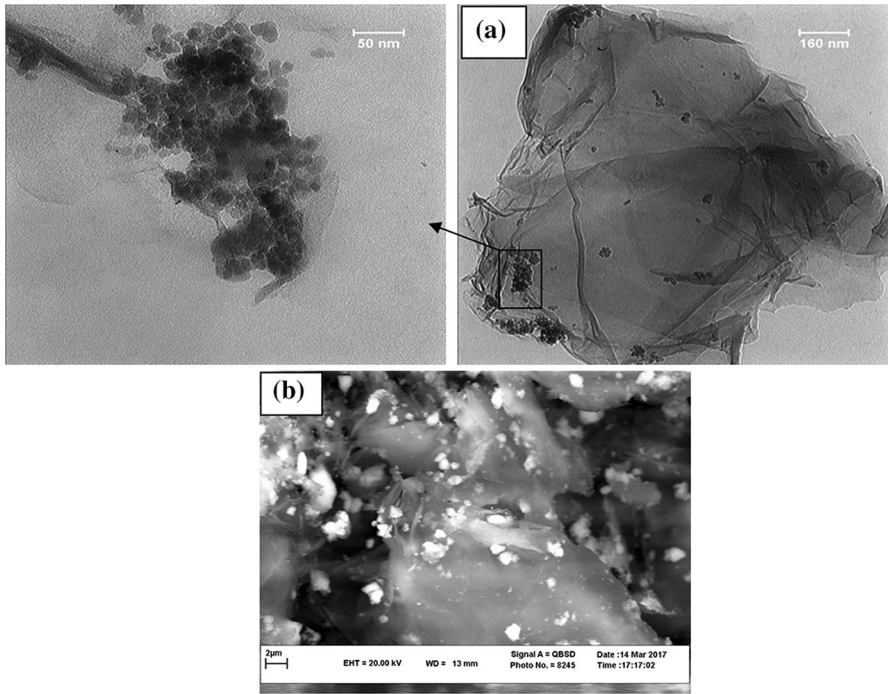


Fig. 2 **a** TEM images of GO-Fe₃O₄ nanocomposite (MGO-1 sample) at two magnifications, **b** SEM image of GO-Fe₃O₄ nanocomposite (MGO-1)

MGO-1

Element	Weight%	Atomic%
CK	49.65	63.36
OK	33.40	31.99
Fe K	16.95	4.65
Totals	100.00	

MGO-3

Element	Weight%	Atomic%
CK	68.23	75.91
OK	27.66	23.11
Fe K	4.10	0.98
Totals	100.00	

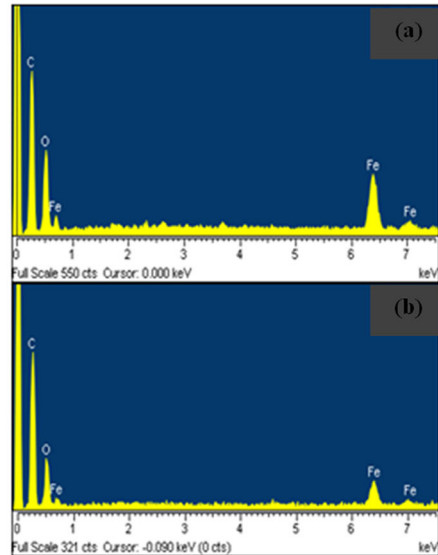


Fig. 3 EDS analysis of GO-Fe₃O₄ nanocomposites at two ratios of GO to Fe₃O₄

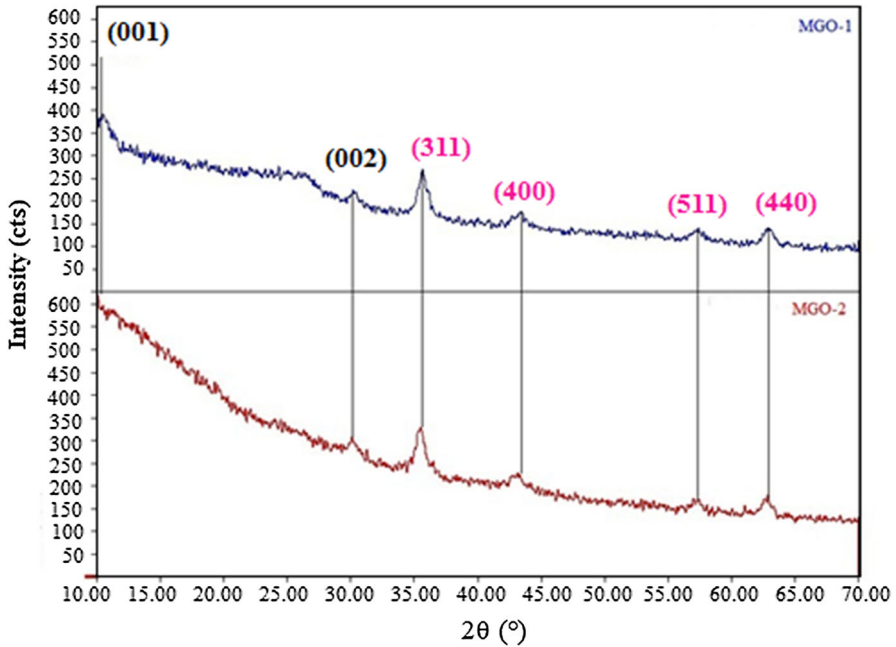


Fig. 4 XRD spectra of GO-Fe₃O₄ nanocomposites obtained using two ratios of GO to Fe₃O₄

stated by Mandal and Chattopadhyay [34], the intensity of diffraction peaks of iron oxide may be reduced due to formation of a GO-Fe₃O₄ composite compared with pure Fe₃O₄. However, there is no clear difference between the XRD spectra of the two samples. The same effect was observed by Jusin et al. [49].

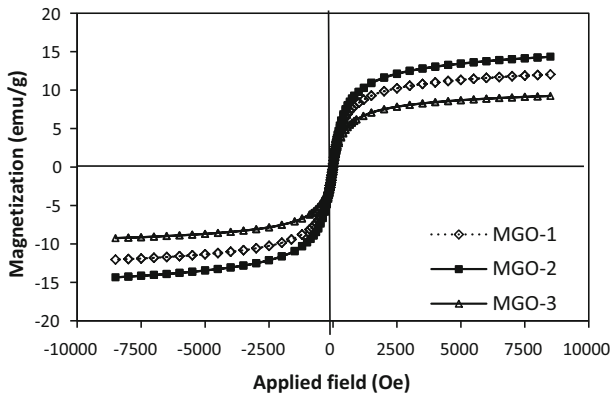


Fig. 5 Magnetization curves of as-prepared GO-Fe₃O₄ nanocomposites

Magnetic property of as-prepared nanocomposite

Vibrating-sample magnetometry was used to measure the magnetization curves of the as-prepared nanocomposites in the range of $-10,000$ to $10,000$ Oe. Figure 5 illustrates the hysteresis loop of magnetization (M , emu/g) versus magnetic field (H , Oe). As can be seen, the saturation magnetization (M_s) was 15, 12, and 9 emu/g for MGO-2, MGO-1, and MGO-3, respectively. Note also that these M_s values of the as-prepared samples are less than that for pure Fe_3O_4 due to the composite structure of the magnetic GO materials. Additionally, the remanent magnetization was found to be about zero for all samples.

The obtained values show that all the samples exhibited supermagnetic properties. From these results, it is obvious that lower Fe_3O_4 loading led to lower magnetic strength. Moreover, at the same magnetite loading, higher magnetic property was observed for MGO-2, which was produced at higher temperature. This trend is consistent with the FTIR results, which confirm greater interaction between GO and Fe_3O_4 . As stated above, NH_2 group of functionalized magnetite can covalently bond to tannic acid-functionalized GO via the OH group of its aromatic section. Such covalent bonding occurs more efficiently at higher temperature. In the case of MGO-2, a higher mixing temperature was applied compared with MGO-1 but at the same ratio of GO to Fe_3O_4 . Therefore, the number and strength of Fe_3O_4 -GO bonds will increase.

TGA results

The composition of the magnetic catalysts was analyzed using TGA; the resulting spectra for both GO and MGO-2 are presented in Fig. 6. As shown in this figure, for GO, weight loss occurred in three steps. The weight loss below 100°C corresponds to evaporation of adsorbed water. Decomposition of oxygen-containing functional groups of GO at 183°C led to 29% weight loss. Up to 600°C , about 98% weight loss was observed, due to decomposition of GO. In the case of MGO-2, the decomposition temperature changed to 191°C with about 53% weight loss up to 800°C , which can be assigned to the Fe_3O_4 composition.

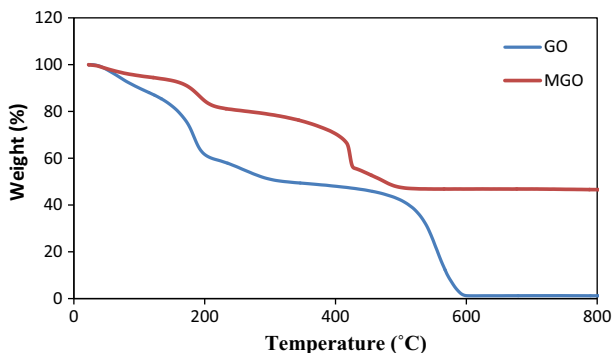


Fig. 6 TGA results for GO and MGO

Catalytic activity of GO-Fe₃O₄ nanocomposite

The applicability of the as-prepared nanocomposite was investigated using the hydrolysis reaction of a synthesized nitropyrimidine compound with excess NaBH₄. For this purpose, MGO-2 was used due to its appropriate magnetic property and Fe-GO connection. 2,4-Dichloro-6-methyl-5-nitropyrimidine was conveniently synthesized according to the published procedure [25]. The nitro group of this compound was reduced by treatment with GO-Fe₃O₄ nanocomposite at room temperature to give 2,4-dichloro-6-methylpyrimidin-5-amine (Scheme 2).

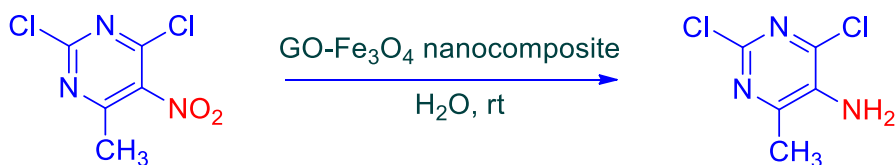
As there is no side reaction during reduction of the nitro compound, UV-Vis absorption spectroscopy can potentially be used to probe the time dependence of the reaction progress. As stated above, sampling from the reaction mixtures was carried out at specified time intervals. The UV-Vis spectra of diluted solutions of nitropyrimidine compound as reactant and product are depicted in Fig. 7. This figure reveals that aqueous solution of 2,4-dichloro-5-nitro-6-methylpyrimidine showed two λ_{max} signals at 210 and 265 nm. However, for samples of the reaction mixture at different times, new peaks were seen at around 235 and 313 nm. These peaks increased with increasing reaction time, implying that a reaction took place.

To investigate the effect of the catalyst dose on the reaction time, the aminolysis reaction was also performed at 1, 3, 5, and 7 mg with fixed amount of other components. The resulting UV-Vis absorption curves are shown in Fig. 8.

As expected, on increasing the nanocatalyst dose, the reaction time decreased from about 20 min for 1 mg catalyst to about 5 min for 7 mg catalyst. It can be concluded that there was no change in the UV spectra between the last two time intervals. It should also be stated that reduction of nitropyrimidine is kinetically restricted when no catalyst is present in the reaction medium.

To confirm reaction completion, two samples using each catalyst dose were taken at the two last intervals and analyzed by TLC without dilution with chloroform/methanol mixture (10:1) as eluent. Figure 8 shows the TLC results for the extracted product compared with the reactant. As can be seen, the spot which featured the product can be clearly distinguished from the reactant by TLC (Fig. 9).

These results show that a small amount of magnetic GO catalyst assisted production of the mentioned aminopyrimidine at room temperature. Note also that water was used as green solvent for the reaction medium. As stated by Li et al. [49], GO has high adsorptive capacity for nitro compounds such as nitrophenol due to hydrogen bonding, hydrophobic interactions, and π - π interactions of their functional groups. On the other hand, Fe₃O₄ has high catalytic capability for



Scheme 2 Reduction reaction of 2,4-dichloro-6-methyl-5-nitropyrimidine to 2,4-dichloro-6-methylpyrimidin-5-amine in presence of GO-Fe₃O₄ nanocomposite

Fig. 7 UV–Vis absorption spectra of reactant (nitropyrimidine) and product (aminopyrimidine)

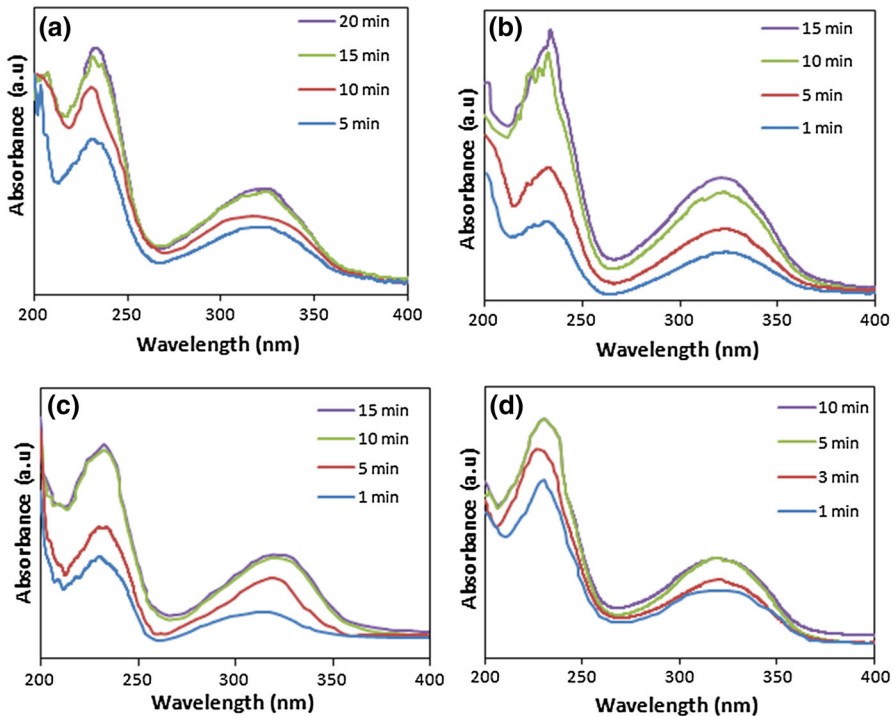
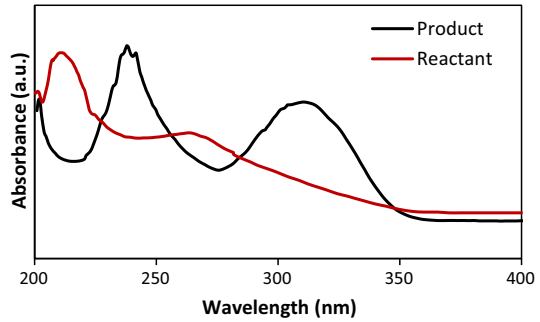


Fig. 8 UV–Vis absorption spectra of reduction reaction at different doses of GO–Fe₃O₄ nanocomposite as catalyst: **a** 1 mg, **b** 3 mg, **c** 5 mg, and **d** 7 mg (25 °C)

reduction of nitro compounds. However, Fe₃O₄ nanoparticles tend to agglomerate. Their attachment to GO can result in enhanced catalytic activity of the nanocomposite catalyst due to the decreased agglomeration effect.

To confirm the superiority of the as-prepared nanocatalyst, the reaction time, catalyst dose, and reaction medium used in this study were compared with the best results of other researchers for the same nitro compounds, as summarized in Table 2. In addition, literature results from previous investigations into the catalytic

Fig. 9 TLC results of 2,4-dichloro-6-methyl-5-aminopyrimidine as product and 2,4-dichloro-6-methyl-5-nitropyrimidine as reactant [chloroform/methanol mixture (10:1) as eluent]

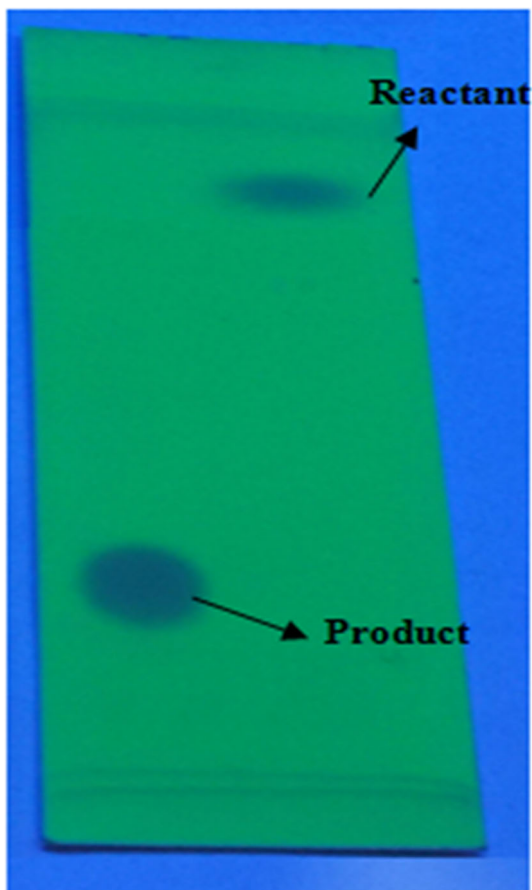


Table 2 Comparison of performance of catalyst introduced in this study with literature results

Catalyst	Temperature (°C)	Solvent	$m_{\text{catalyst}}/m_{\text{reactant}}$ (g/g)	Reaction time (min)	Ref.
Magnetic GO	25	Water	0.067–0.47	20–5	This study
Fe–Ni	50	Water	2.32	10	[4]
Fe	25	Acetic acid	1.19	120	[40]
Magnetic GO ^a	98	Ethanol	0.041	17	[51]

^aReaction data for aniline reduction

activity of magnetic GO for reduction of other nitro compounds were compared with the results of this study.

As reported by Karimian et al. [40], when Fe was used as catalyst to produce aminopyrimidine from nitropyrimidine, the time required for reaction completion exceeded 2 h. However, Rezazadeh et al. [4] reported that use of a reaction mixture including bimetallic Fe–Ni as nanocatalyst at 90 °C could reduce the reaction time to 10 min. However, high temperature was required when this highly active bimetallic catalyst was utilized in the reaction medium. The low reaction time, temperature, and catalyst dose herein indicate that GO–Fe₃O₄ is a unique candidate for production of this intermediate compound.

Confirmation of product structure via spectroscopic and microanalytical data

Spectroscopic and microanalytical data confirmed reduction of the nitro group of 2,4-dichloro-6-methyl-5-nitropyrimidine to 2,4-dichloro-6-methylpyrimidin-5-amine; For instance, the FTIR spectrum of compound 2,4-dichloro-6-methylpyrimidin-5-amine showed definite stretching vibration bands at ν of 3472 and 3371 cm⁻¹, indicating presence of NH₂ group in the product. The vibration band at ν of 1621 cm⁻¹ corresponds to C=N of pyrimidine ring. The FTIR spectra of 2,4-Dichloro-6-methyl-5-nitropyrimidine and 2,4-dichloro-6-methylpyrimidin-5-amine are compared in Figs. 10 and 11. The ¹H NMR spectrum of the synthesized compound showed the signal of methyl group of pyrimidine moiety at δ of 2.32 ppm and a D₂O exchangeable signal at δ 6.20 ppm belonging to NH₂ group. The mass spectrum also showed the molecular ion peak of the compound at m/z of

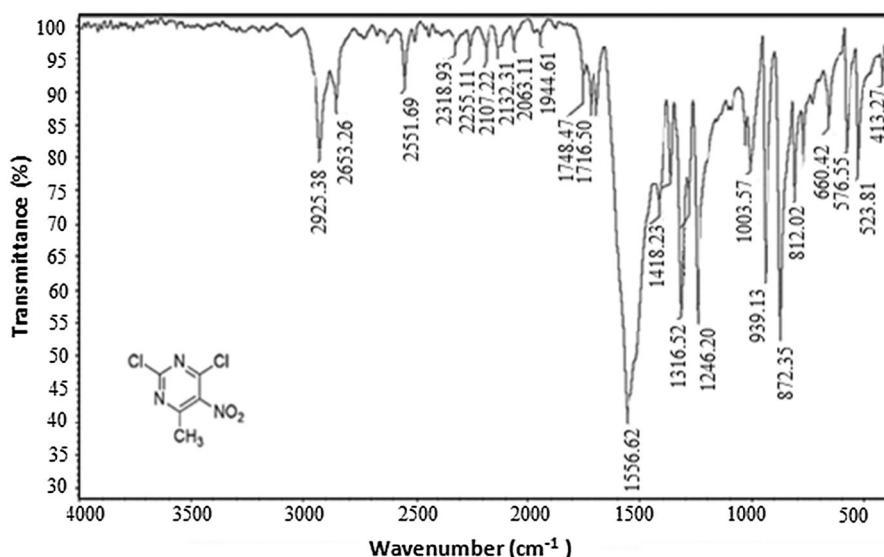


Fig. 10 FTIR spectrum of 2,4-dichloro-6-methyl-5-nitropyrimidine

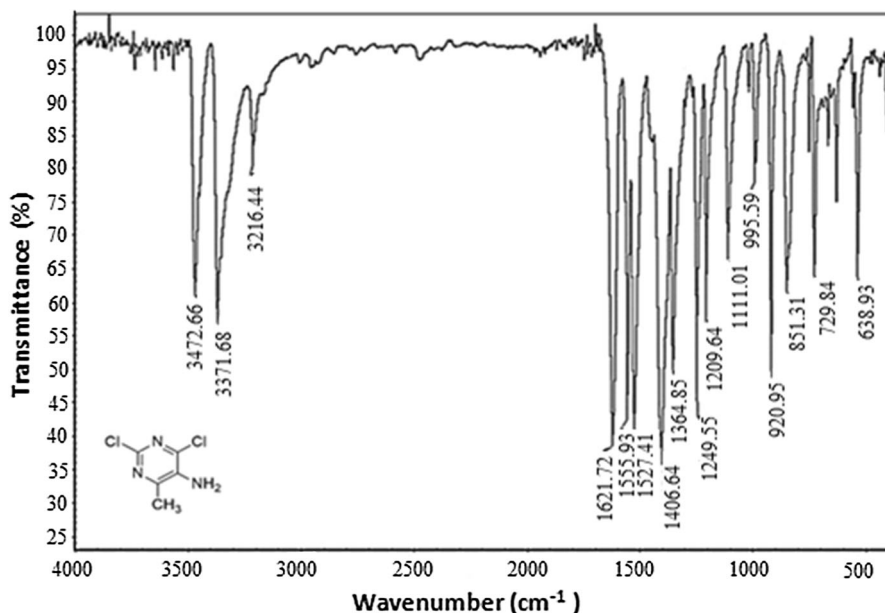


Fig. 11 FTIR spectrum of 2,4-dichloro-6 methylpyrimidin-5-amine

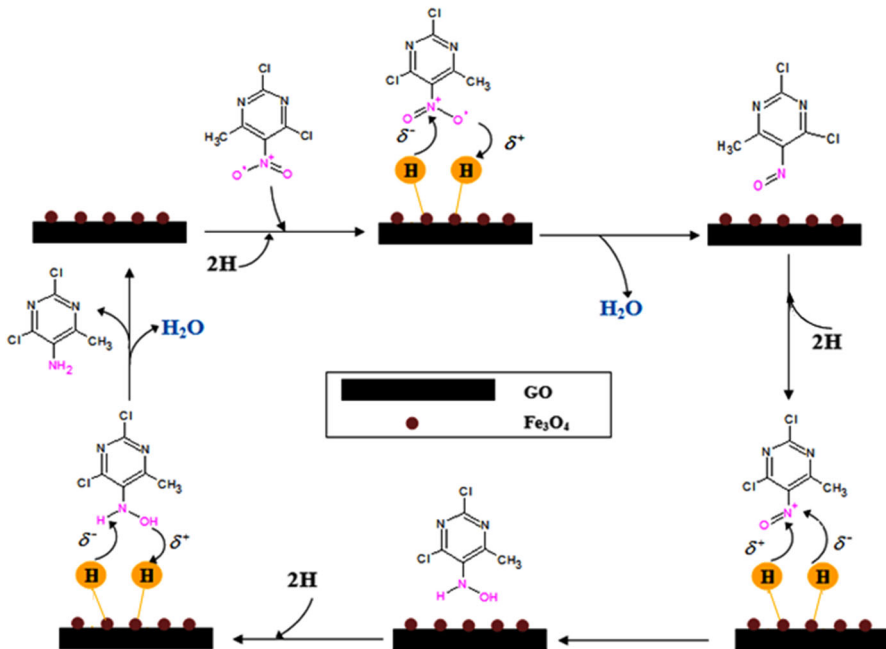
178 (M^+), corresponding to the molecular formula $C_5H_5Cl_2N_3$. Elemental analysis also confirmed the molecular formula of this compound.

Reaction mechanism

The reduction of nitropyrimidine by $NaBH_4$ in presence of $GO-Fe_3O_4$ nanocomposite as catalyst may proceed according to a mechanism suggested by Verakumar et al. [50] (Scheme 3). Firstly, BH_4^- reacts with Fe_3O_4 nanoparticles, and metal hydride is generated on the surface of the catalyst. Simultaneously, nitropyrimidine molecules adsorb on the surface of the catalyst. Nitroso compound and water molecules are the product of this step. Then, nitroso compound reacts with more hydrogen molecules to form hydroxyl amine. Subsequently, hydroxyl amine group is converted to amine group, and finally aminopyrimidine is produced with water as byproduct.

Conclusions

Magnetic GO nanocomposite was prepared by a new method and employed as catalyst for production of 2,4-dichloro-6 methylpyrimidin-5-amine as an intermediate compound for use in drug synthesis. Amino-functionalized Fe_3O_4 was covalently bonded to GO using tannic acid as binder. As-prepared nanocomposites obtained under different synthesis conditions were characterized by FTIR, XRD, TEM, SEM, EDS, and VSM. The results showed that synthesis using GO/Fe_3O_4



Scheme 3 Suggested mechanism for reduction of nitropyrimidine compound in presence of borohydride and GO-Fe₃O₄ nanocatalyst

ratio of 1:1 (w/w) at 50 °C resulted in higher magnetic strength and GO-Fe₃O₄ interactions. The catalytic activity of the optimal GO/Fe₃O₄ nanocomposite was then investigated in reduction of 2,4-dichloro-6-methyl-5-nitropyrimidine. Probing of the reaction medium via UV-Vis absorption spectroscopy and TLC analysis revealed that the reaction completed after 10 min. According to the results, the as-prepared magnetic GO catalyst has the ability to reduce nitropyrimidine to aminopyrimidine. These unique advantages, including green (aqueous) reaction medium, low reaction temperature, and rapid reaction, make GO/Fe₃O₄ a special candidate for production of aminopyrimidines.

References

1. M. Esfahanizadeh, S. Mohebbi, B.D. Bozorg, S. Amidi, A. Gudarzi, S.A. Ayatollahi, F. Kobarfard, *Iran J. Pharm. Res.* **14**(2), 417 (2015)
2. E.Y. Schmidt, I.V. Tatarinova, N.I. Protsuk, I.A. Ushakov, B.A. Trofimov, *J. Org. Chem.* **82**(1), 119 (2017)
3. S. Chandrappa, K. Vinay, T. Ramakrishnappa, K.S. Rangappa, *Synlett* **20**, 3019 (2010)
4. S. Rezaeadeh, B. Akhlaghinia, E.K. Goharshadi, H. Sarvari, *J. Chin. Chem. Soc.* **61**, 1108 (2014)
5. P. Serna, P. Concepcin, A. Corma, *J. Catal.* **265**(1), 19 (2009)
6. Y. Yamane, X. Liu, A. Hamasaki, T. Ishida, M. Haruta, T. Yokoyama, M. Tokunaga, *Org. Lett.* **11**(22), 5162 (2009)
7. C. Su, M. Acik, K. Takai, J. Lu, S.J. Hao, Y. Zheng, P. Wu, Q. Bao, T. Enoki, Y.J. Chabal, K.P. Loh, *Nat. Commun.* **3**, 1298 (2012)
8. A. Lerf, H.Y. He, M. Forster, J. Klinowski, *J. Phys. Chem. B* **102**, 4477 (1998)

9. H. He, C. Gao, *ACS Appl. Mater. Interfaces* **2**, 3201 (2010)
10. D.C. Marcano, D.V. Kosynkin, J.M. Berlin, A. Sinitskii, Z.Z. Sun, A. Slesarev, L.B. Alemany, W. Lu, J.M. Tour, *ACS Nano* **4**, 4806 (2010)
11. W. Fan, W. Gao, C. Zhang, W.W. Tjiu, J. Pan, T. Liu, *J. Mater. Chem.* **22**(48), 25108 (2012)
12. J.H. Yang, B. Ramaraj, K.R. Yoon, *J. Alloys Compd.* **583**, 128 (2014)
13. V.K. Rana, M.-C. Choi, J.-Y. Kong, G.Y. Kim, M.J. Kim, S.-H. Kim, S. Mishra, R.P. Singh, C.-S. Ha, *Macromol. Mater. Eng.* **296**, 131 (2011)
14. Y.S. Huang, Y.J. Lu, J.P. Chen, *J. Magn. Magn. Mater.* **427**, 34 (2017)
15. L. Cui, Y. Wang, L. Gao, L. Hu, L. Yan, Q. Wei, B. Du, *Chem. Eng. J.* **281**, 1 (2015)
16. M.A. Farghali, T.A.S. El-Din, A.M. Al-Enizi, R.M. El Bahnasawy, *Int. J. Electrochem. Sci.* **10**, 529 (2015)
17. V.K. Gupta, N. Atar, M.L. Yola, Z. Ustundag, L. Uzun, *Water Res.* **48**, 210 (2014)
18. R. Xu, H. Bi, G. He, J. Zhu, H. Chen, *Mater. Res. Bull.* **57**, 190 (2014)
19. H.A. Elazab, A.R. Siamaki, S. Moussa, B.F. Gupton, M.S. El-Shall, *Appl. Catal. A. General* **491**, 58 (2015)
20. L. Gao, C. Lian, Y. Zhou, L. Yan, Q. Li, C. Zhang, L. Chen, K. Chen, *Biosens. Bioelectron.* **60**, 22 (2014)
21. T. Ramanathan, A.A. Abdala, S. Stankovich, D.A. Dikin, M. Herrera-Alonso, R.D. Piner, D.H. Adamson, H.C. Schniepp, X. Chen, R.S. Ruoff, S.T. Nguyen, I.A. Aksay, R.K. Prud'homme, L.C. Brinson, *Nat. Nanotechnol.* **3**, 327 (2008)
22. H. Bai, C. Li, G.Q. Shi, *Adv. Mater.* **23**, 1089 (2011)
23. X.M. Chen, G.H. Wu, J.M. Chen, X. Chen, Z.X. Xie, X.R. Wang, *J. Am. Chem. Soc.* **133**, 3693 (2011)
24. R. Sibirian, T. Kondo, J. Nakamura, *J. Phys. Chem. C* **117**, 3635 (2013)
25. Q. Lu, W. Wei, Z.X. Zhou, Z.X. Zhou, Y.J. Zhang, S.Q. Liu, *Analyst* **139**, 2404 (2014)
26. D.P. Yu, J.F. Yao, L. Qiu, Y.Z. Wu, L.X. Li, Y. Feng, Q. Liu, D. Li, H.T. Wang, *RSC Adv.* **3**, 11552 (2013)
27. H. Zhang, X. Lv, Y. Li, Y. Wang, J. Li, *ACS Nano* **4**, 380 (2010)
28. L.S. Zhang, L.Y. Jiang, H.J. Yan, W.D. Wang, W. Wang, W.G. Song, Y.G. Guo, L.J. Wan, *J. Mater. Chem.* **20**, 5462 (2010)
29. F.A. He, J.T. Fan, D. Ma, L.M. Zhang, C. Leung, H.L. Chan, *Carbon* **48**, 3139 (2010)
30. A. Hassani, G. Çelikdağ, P. Eghbali, M. Sevim, S. Karaca, Ö. Metin, *Ultrason. Sonochem.* **40**, 841 (2018)
31. M.Y. Lim, Y.S. Choi, J. Kim, K. Kim, H. Shin, J.J. Kim, D.M. Shin, J.C. Lee, *J. Membr. Sci.* **521**, 1 (2017)
32. N. Huang, M. Liu, M. Li, Y. Zhang, S. Yao, *Anal. Chim. Acta* **853**, 249 (2015)
33. J. Huang, Q. Chang, Y. Ding, X. Han, H. Tang, *Chem. Eng. J.* **254**, 434 (2014)
34. P. Mandal, A.P. Chattopadhyay, *Dalton Trans.* **25**, 11444 (2015)
35. X. Yang, X. Zhang, Y. Ma, Y. Huang, Y. Wang, Y. Chen, *J. Mater. Chem.* **19**, 2710 (2009)
36. G. Xi, P. Xi, H. Liu, F. Chen, L. Huang, Z. Zeng, *J. Mater. Chem.* **22**(3), 1033 (2012)
37. P. Shi, N. Ye, *Anal. Methods* **6**, 9725 (2014)
38. H. Teymourian, A. Salimi, S. Khezrian, *Biosens. Bioelectron.* **49**, 1 (2013)
39. H. Li, Z. Chi, J. Li, *Desalin. Water Treat.* **52**(10–12), 1937 (2014)
40. A. Karimian, H. Eshghi, M. Bakavoli, A. Shiri, *Heterocycl. Commun.* **20**(5), 275 (2014)
41. G. He, H. Chen, J. Zhu, F. Bei, X. Sun, X. Wang, *J. Mater. Chem.* **21**, 14631 (2011)
42. H. Chen, M.B. Müller, K.J. Gilmore, G.G. Wallace, D. Li, *Adv. Mater.* **20**, 3557 (2008)
43. G.H. Sayed, F.M. Ghuiba, M.I. Abdou, E.A.A. Badr, S.M. Tawfik, N.A.M. Negm, *Colloid Surf. A* **393**, 96 (2012)
44. R.M. Silverstein, G.C. Bassler, T.C. Morrill, *Spectrometric Identification of Organic Compounds* (Wiley, New York, 1981)
45. M.N. Batin, V. Popescu, *Powder Metall. Prog.* **11**, 201 (2011)
46. M.Y. Lim, Y.S. Choi, J. Kim, K. Kim, H. Shin, J.J. Kim, D.M. Shin, J.C. Lee, *J. Membrane Sci.* **521**, 1 (2017)
47. S. Sakaguchi, T. Kubo, Y. Ishii, *Angew. Chem. Int. Ed.* **40**(13), 2534 (2001)
48. J.W. Jusin, M. Aziz, G.P. Sean, J. Jaafar, *Malays. J. Anal. Sci.* **20**(1), 149 (2016)
49. J. Li, D. Kuang, Y. Feng, F. Zhang, Z. Xu, M. Liu, *J. Hazard. Mater.* **201–202**, 250 (2012)
50. P. Veerakumar, M. Velayudham, K.L. Lu, S. Rajagopal, *Appl. Catal. A: General* **439–440**, 197 (2012)
51. G. He, W. Liu, X. Sun, Q. Chen, X. Wang, H. Chen, *Mater. Res. Bull.* **48**, 1885 (2013)